Recent Fourier continuation-based solvers for time-dependent problems in solids, fluids & their interactions

Faisal Amlani

CSMA 2022
15ème Colloque National en Calcul des Structures
16-20 Mai 2022, Presqu'île de Giens (Var)

Recent Fourier continuation-based solvers for time-dependent problems in solids, fluids & their interactions

F. Amlani[1,2]

[1] *CNRS, LMT, École Normale Supérieure Paris-Saclay, Université Paris-Saclay, France, famlani@gmail.com*
[2] *Department of Aerospace & Mechanical Engineering, University of Southern California, USA*

Résumé — This contribution overviews a spectral methodology for the numerical solution of partial differential equation systems governing various mechanical wave propagation problems. Based on a Fourier continuation (FC) approach for the accurate trigonometric interpolation of a non-periodic function, such a high-order algorithm produces solutions with essentially no numerical dispersion ; possesses mild CFL constraints scaling only linearly with spatial discretization sizes ; and parallelizes efficiently for high-performance. Applications to non-destructive testing, blood dynamics, and geophysics are discussed.
Mots clés — (pseudo)spectral methods, wave propagation, fluid-structure interactions, non-destructive testing, hemodynamics, tsunami generation

1 Introduction

Fourier continuation (FC) methods produce highly-accurate Fourier series representations of non-periodic functions while avoiding the well-known Gibb's "ringing effect" [13]. Such techniques expand the applicability of Fourier-based partial differential equation (PDE) solvers towards general (physical) boundary conditions [6, 8, 9] and computational domains [2, 6]. Corresponding solutions provide Fast Fourier Transform- (FFT-)speed high-order accuracy and faithfully capture the dispersion or diffusion characteristics of the underlying continuous problems. A number of both implicit- and explicit-in-time FC-based solvers have been constructed for a variety of physical equations including those for acoustic beams [3], light transport [15], compressible fluids [2], incompressible fluids [14] and (shock-inducing) conservation laws [18].

This work presents on overview of recent developments [5, 6, 7, 8, 9, 10] in certain explicit Fourier continuation-based (pseudo) spectral algorithms (Section 2) that have been motivated by scientific applications (Section 3) in non-destructive testing (for the study of mode conversions in ultrasonic experiments on elastic plates), seismogenic tsunamis (for the study of the tsunami generation potential of strike-slip earthquakes), and cardiovascular hemodynamics (for the study of fluid-structure blood flow waves and their effects on neurodegenerative diseases). Such developments have been driven by subsequent challenges in the treatment of the corresponding equations that respectively govern (linear) elastodynamics, (nonlinear) shallow water wave dynamics (coupled to elastic rupture models) and (nonlinear) fluid-structure arterial wave dynamics (coupled to dynamic heart models). In particular, the algorithms presented here extend the class of FC methods to encompass variable-coefficient 3D systems, general (curved) 3D domains, 3D parallelization, Neumann-like (e.g., traction or convective flux) boundary conditions, and nonlinear/nonstationary (ODE-governed) coupling (e.g., dynamic 0D-coupling). The resulting high-order solvers enjoy a number of desirable properties for scientific computation : accuracy by means of relatively coarse discretizations ; little-to-no numerical dispersion or diffusion errors ; mild (linear) CFL constraints on time integration ; and efficient parallelization for distributed-memory high-performance computing.

2 Fourier continuation methods

For point values $f(x_i)$ of a given smooth function $f(x) : [0,1] \to \mathbb{R}$ defined on a structured uniform discretization $x_i = i\Delta x, i = 0,\ldots,N-1$, $\Delta x = 1/(N-1)$, the FC method constructs a fast-converging

interpolating trigonometric polynomial (Fourier series representation) $f_{\text{cont}} : [0,b] \to \mathbb{R}$ on a region $[0,b]$ that is slightly larger than the original physical domain od definition $[0,1]$:

$$f_{\text{cont}} = \sum_{k=-M}^{M} a_k e^{\frac{2\pi i k x}{b}} \quad \text{s.t. } f_{\text{cont}}(x_i) = f(x_i),\ i = 0,...,N-1, \tag{1}$$

where $M = (N + N_{\text{cont}})/2$ is a bandwidth parameter for a number of points N_{cont} added to the original domain (such that $b = (N + N_{\text{cont}})\Delta x$)). The FC function f_{cont} renders the original function f discretely periodic, i.e., f_{cont} approximates f to high-order in the original domain $[0,1]$ and is approximately periodic on the slightly larger domain $[0,b]$, $b > 1$. Spatial derivatives of a PDE can then be produced by exact termwise differentiation of this series as

$$\frac{\partial f_{\text{cont}}}{\partial x}(x) = \sum_{k=-M}^{M} \left(\frac{2\pi i k}{b}\right) a_k e^{\frac{2\pi i k x}{b}}. \tag{2}$$

This ultimately provides the numerical derivatives of f to high-order by restricting the domain of $\partial f_{\text{cont}}/\partial x$ to the original unit interval. Hence the approximation rests in the construction of (1) from which the computation of the derivative (2) can be facilitated by the Fast Fourier Transform (FFT). Note here that f has been defined on $[0,1]$ without loss of generality.

2.1 Accelerated Fourier continuation : FC(Gram)

The coefficients a_k of (1) are found in the most intuitive treatment [12] via the solution to the least squares problem given by

$$\min_{a_k} \sum_{i=0}^{N-1} |f_{\text{cont}}(x_i) - f(x_i)|^2 \tag{3}$$

by the Singular Value Decomposition (SVD). This can become rather costly for 3D problems as well as time-dependent solutions of complex boundary-valued PDEs (where each spatial dimension requires application of SVDs at each timestep). An accelerated method [2, 6], known as FC(Gram), can circumvent such expense by employing small vectors of only a handful of function values near the left and right endpoints at $x = 0$ and $x = 1$ which can then be projected onto a Gram polynomial basis (whose continuations are precomputed through solving the corresponding least squares problem (3) by high-precision SVD). That is, one utilizes a subset of the given function values on small numbers d_ℓ and d_r of matching points $\{x_0,..,x_{d_\ell-1}\}$ and $\{x_{N-d_r},...,x_{N-1}\}$ contained in small subintervals on the left and right ends of the interval $[0,1]$ to produce a discrete periodic extension of size N_{cont}. This is accomplished by projecting these end values onto a Gram basis up to degree $d_\ell - 1$ (or $d_r - 1$) of polynomials (producing a polynomial interpolant) whose FC extensions are precomputed and whose orthogonality is enforced by the natural discrete scalar product defined by the discretization points. This effectively forms a “basis" of continuation functions with which to quickly and accurately extend the given function f to provide a smooth transition from $f(x = 0)$ back to $f(x = 1)$ over the interval $[0,b]$.

Defining the vectors of matching points for the left and right as

$$\mathbf{f}_\ell = (f(x_0), f(x_1), ..., f(x_{d_\ell-1}))^T, \quad \mathbf{f}_r = (f(x_{N-d_r}), f(x_{N-d_r+1}), ..., f(x_{N-1}))^T, \tag{4}$$

the continuation operation can be expressed in a block matrix form as

$$\mathbf{f}_{\text{cont}} = \begin{bmatrix} \mathbf{f} \\ A_\ell Q_\ell^T \mathbf{f}_\ell + A_r Q_r^T \mathbf{f}_r \end{bmatrix}, \tag{5}$$

where $\mathbf{f} = (f(x_0), \ldots, f(x_{N-1}))^T$ is a column vector containing the discrete point values of f; $\mathbf{f}_{\text{cont}}$ is a vector of the $N + N_{\text{cont}}$ continued function values; I is the $N \times N$ identity matrix; and A_ℓ, A_r contain the corresponding N_{cont} values that perform the continuation from the left and the right (such that the sum of leftward and rightward continuations provides the necessary smooth transition). The columns of Q_ℓ, Q_r contain the d_ℓ, d_r point values of each element of the corresponding Gram polynomial basis (produced from a QR decomposition of a Vandermonde matrix), and can be modified [6, 10] to match derivatives

at endpoints (e.g., $\mathbf{f}_\ell = (f(x_0), f(x_1), ..., f(d_\ell - 1), \partial f/\partial x(x_{d_\ell}))^T$) for Neumann boundary conditions. Figure 1 illustrates an example Fourier continuation of a non-periodic function. The resulting continued vector $\mathbf{f}_{\text{cont}}$ can be interpreted as a set of discrete values of a smooth and periodic function that can be approximated to high-order via FFT on an interval of size $(N+N_{\text{cont}})\Delta x$. For the solvers [5, 6, 7, 8, 9, 10] reviewed in this work, $N_{\text{cont}} = 25$ and $d_\ell, d_r = 5$ at physical boundaries.

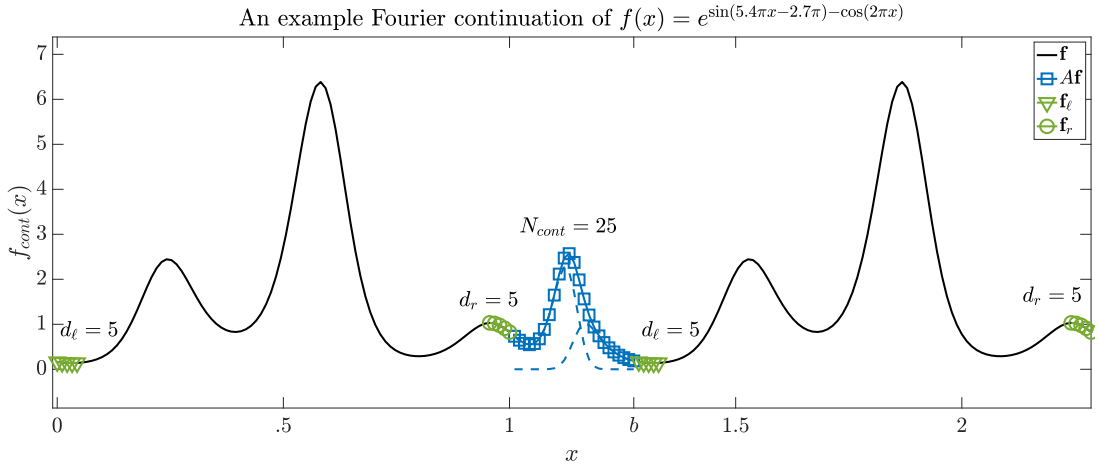

FIGURE 1 – An example Fourier continuation from [8] of a non-periodic function. The original function on $[0, 1]$ is translated by a distance of length $N_{\text{cont}}\Delta x$ whose values are filled-in by the sum of "blend-to-zero" continuations (dashed lines) in order to render the function periodic. Triangles and circles represent the discrete $d_\ell, d_r = 5$ matching points, and squares represent the discrete $N_{\text{cont}} = 25$ continuation points that comprise the extension.

2.2 Curved geometries & parallel domain decompositions

For general physical domains, realistic curved geometries can be treated by an overset method decomposing the computational domain Ω into a union $\Omega = \bigcup_j \Omega_j$ of a finite number of overlapping, boundary-conforming patches which are endowed with uniform Cartesian-like discretizations within each one of which a curvilinear formulation of the PDE of interest is evolved [6]. Additionally, a decomposition of each curvilinear patch Ω_j into mutually disjoint subpatches enables a parallelization for distributed-memory environments through which some solvers have achieved nearly perfect scalability [4, 6]. For each (sub)patch, the governing equations must be solved in a curvilinear form, which can be obtained by considering the chain rule expression

$$\nabla_{\mathbf{q}} = [J_{\mathbf{x}}(\mathbf{q})]^T \nabla_{\mathbf{x}}, \tag{6}$$

where $(J_{\mathbf{x}}(\mathbf{q}))_{ij} = \partial x^i/\partial q^j$ is the Jacobian matrix of the given mapping $\mathbf{x}(\mathbf{q})$. Provided $\det((J_{\mathbf{x}})(\mathbf{q}))$ does not vanish, inversion of this linear system gives the expression

$$\nabla_{\mathbf{x}} = \left[(J_{\mathbf{x}}(\mathbf{q}))^{-1}\right]^T \nabla_{\mathbf{q}} = [J_{\mathbf{q}}(\mathbf{x})]^T \nabla_{\mathbf{q}}, \tag{7}$$

where the last equality results from the reverse chain rule formula $\nabla_{\mathbf{x}} = [J_{\mathbf{q}}(\mathbf{x})]^T \nabla_{\mathbf{q}}$. Thus the derivatives $\partial q^i/\partial x^j$ can be produced in terms of the derivatives of the given mapping $\partial x^i/\partial q^j$ (computed analytically, if known, or via a seperate application of FC). Absorbing boundary conditions can also be constructed from such overset curvilinear strategies [4].

2.3 High-order time integration

FC-based solvers can be completed by any suitable time integration scheme. Those presented in Section 3 employ explicit timestepping via fourth-order Adams-Bashforth methods, yielding mild, linearly scaling CFL constraints on the time discretization [5, 6, 8, 9]. Such high-order timestepping has proven to

be particularly useful for coupling with 0D ordinary differential equation- (ODE-)based boundary conditions (such as with the heart models of [8, 9, 17]). Other explicit timesteppers can be used, including the fourth-order Runge-Kutta (RK4) method. Both methods provide adequate regions of absolute stability, but each timestep for RK4 entails four evaluations of the right-hand-side (which can be burdensome for 3D calculations), and enforcement of boundary conditions at intermediate RK steps may be problematic (especially for time-dependent boundary conditions).

3 Scientific applications

The following examples demonstrate the efficacy of FC-based numerical algorithms in constructing physically-faithful and high-fidelity simulated solutions for problems in solids (elastodynamics), fluids (shallow water wave dynamics) and their interactions (cardiovascular hemodynamics). Such solvers have been validated against data ranging from on the order of seconds (coarse, natural data of tsunami wave observations) to on the order of microseconds (finely-controlled experimental data of ultrasonic non-destructive testing experiments).

3.1 Non-destructive testing

Ultrasonic NDT is a powerful tool to study the integrity of a variety of plate-like and beam-like structures from aircraft wings to oil pipelines to bridges. Low-energy, high-frequency wave packets are introduced into a material to determine fundamental properties (e.g., elastic constants) or to detect defects (e.g., cracks or holes) by measuring and analyzing the propagation, reflection and attenuation of incident pulses. These pulses are excited by a certain combination of pressure and shear wave modes to enable propagation of a single guided wave. Subsequent wave dynamics and scattering patterns can then be used to extract important features—such as the positions, dimensions and orientations of defects—by solving the corresponding direct or inverse problems.

The dynamics of ultrasonic (1Mhz to 10Mhz) vibrations excited in such structures can be modeled as elastic waves in a linear, isotropic, possibly heterogeneous 3D medium, which are governed by the PDE system

$$\rho(\mathbf{x})\frac{\partial^2 \mathbf{u}}{\partial t^2}(\mathbf{x},t) = \nabla\cdot\left[\mu(\mathbf{x})\left(\nabla\mathbf{u}(\mathbf{x},t)+\nabla\mathbf{u}^T(\mathbf{x},t)\right)+\lambda(\mathbf{x})\left(\nabla\cdot\mathbf{u}(\mathbf{x},t)\right)I\right]+\mathbf{f}(\mathbf{x},t), \quad \mathbf{x}\in\Omega\subset\mathbb{R}^3, \quad t\geq t_0 \tag{8}$$

for a general 3D domain $\Omega\in\mathbb{R}^3$; position $\mathbf{x}$ and time-dependent displacement $\mathbf{u}(\mathbf{x},t)$; body force vector $\mathbf{f}(\mathbf{x},t)$; and spatially-varying material properties specified by Lamé parameters $\mu(\mathbf{x}),\lambda(\mathbf{x})$ and density $\rho(\mathbf{x})$. In an effort to model certain ultrasonic NDT experiments on thin aluminum plates with holes (where a pulsed TV-holography system records the 2D acoustic field of the instantaneous out-of-plane displacement over the surface [16]), an FC-based solver for (8) with traction- (surface-)free boundary conditions on the plate and in the holes (left images of Figure 2) has been recently introduced [6]. The high-order solver invokes curvilinear transformations, overset grid decompositions and high-performance parallelization (up to 512 processing cores). The resulting speed, accuracy and limited numerical dispersion resolves the high-frequency and transient incident pulses of the experimental configuration in reasonable computational times, ultimately providing a systematic quantitative comparison between numerically simulated maps and filtered experimental displacement maps [7]. Results demonstrate very good agreement both in amplitude and phase, including the backscattering zone, which confirms the feasibility and potential of the proposed numerical method for the characterization of experimental transient scattering patterns measured with the pulsed TV-holography technique. The pixel-wise L^2 errors in the colored boxes of Figure 2 fall within 10% error in both amplitude and phase—indicating a “perfect" match within experimental uncertainty [7]. FC simulations have additionally given a first-time look inside defect holes via numerical analysis of all three displacement components (two of which are unobservable with the experimental setup). This has provided insight into a mode conversion during interaction in the thickness of the hole that is not captured by simplified (e.g., time-harmonic and scalar [16]) models.

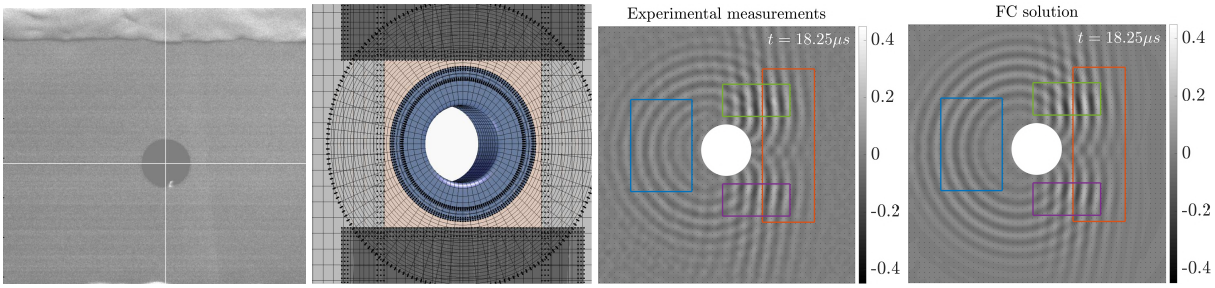

FIGURE 2 – Left to right : a photo of a physical NDT sample and its corresponding 3D overset computational domain from [6] ; temporal snapshots of normalized experimental and FC-simulated displacement fields from [7], simulated on 512 processing cores.

3.2 Seismogenic tsunamis

A magnitude 7.5 earthquake struck Sulawesi, Indonesia in 2018 and triggered disastrous consequences in which hundreds were killed and thousands more displaced. In particular, a devastating tsunami was generated in the nearby Palu bay—an unexpected event due to the predominantly in-plane ground motion produced by strike-slip ruptures such as this earthquake. These motions are not known to excite significant waves (as opposed to large final vertical displacements in subduction zones), and hence the underlying mechanisms behind this tsunami continue to be debated. However, a key notable feature of this earthquake is that it ruptured at supershear speed, i.e., with a rupture velocity greater than the shear wave speed of the host medium. Such supershear ruptures produce two shock fronts (or Mach fronts) that correspond to an exceedance of shear and Rayleigh wave velocities and that carry with them significant and minimally attenuated particle velocities to large distances.

Since tsunamis are conventionally known to occur from large vertical (final, static) displacements, most tsunami solvers treat equations with static bathymetry (topography). In order to understand the effects of supershear earthquake dynamics and to enable sourcing using time-dependent displacement as well as velocity of the ground motion, one can consider a nonlinear version of the (non-dispersive) depth-averaged Euler equations (known as shallow wave equations) incorporating ground dynamics, i.e.,

$$\begin{cases} \dfrac{\partial H}{\partial t} + \nabla \cdot (H\mathbf{u}) = 0, \\ \dfrac{\partial H\mathbf{u}}{\partial t} + \nabla \cdot \left(H\mathbf{u} \otimes \mathbf{u} + \dfrac{1}{2} g H^2 \right) = gH\nabla h, \end{cases} \qquad H = h(\mathbf{x},t) + \eta(\mathbf{x},t), \quad \mathbf{x} \in \Omega \subset \mathbb{R}^2, \quad t \geq t_0 \qquad (9)$$

for depth-averaged velocity $\mathbf{u} = \mathbf{u}(\mathbf{x},t)$, total column height $H = H(\mathbf{x},t)$, tsunami height $\eta(\mathbf{x},t)$ from the free surface, bathymetry (ocean floor topography) $h(\mathbf{x},t)$ and gravitational constant g.

This nonlinear formulation includes time-dependent changes to the vertical ocean floor displacement $h(x,t)$ and, in particular, its vertical velocity $\partial h/\partial t$ (displacement h may be small, but $\partial h/\partial t$ can be large). The ground motion source is generated by a 3D supershear rupture model (using a staggered-grid finite difference method) that agrees with GPS records recorded at a station near the fault. This can be subsequently coupled with a new high-order FC-based dispersionless solver for (9) [5] that can take rapidly varying topography into account without worrying about the discretization details and that is stable when used with the (given) discretization of the dynamic rupture model. This has enabled adequate resolution of the different spatial and temporal scales involved between the supershear source dynamics (on the order of milliseconds) and the corresponding tsunami dynamics (observed on the order of seconds). Remarkably, the simulated tsunami using the FC-based dispersionless numerical model captures the tsunami arrival and the primary dynamics that are given by water heights observed every second from waveforms generated by carefully-calibrated CCTV camera analysis at the Pantoloan tidal station (Figure 3). This is a newly discoverd mechanism/configuration of tsunami-genesis and suggests that consideration of the *speed* of an earthquake may also be important for rapid tsunami hazard assessment [5].

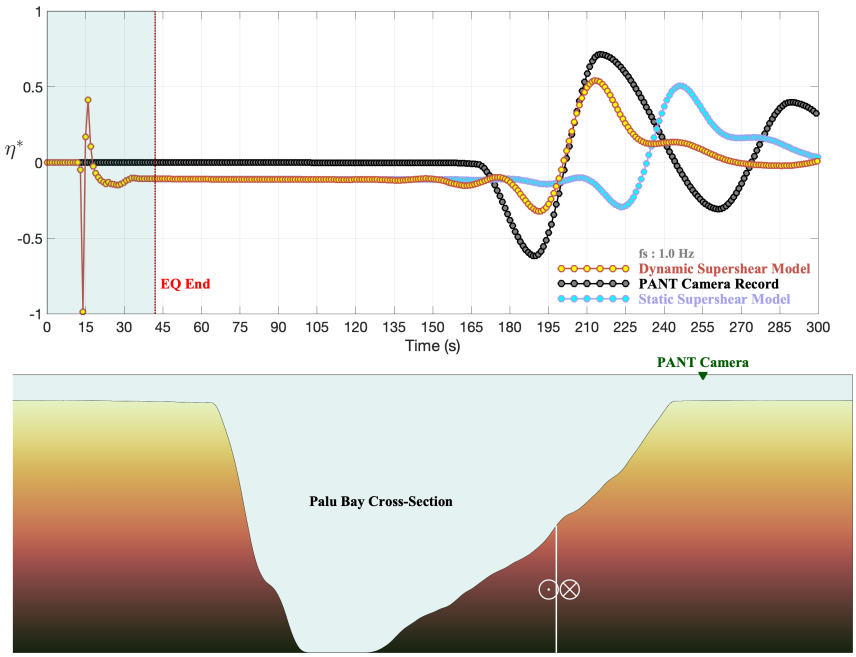

FIGURE 3 – A comparison from [5] of normalized tsunami heights as predicted by FC-based numerical simulations (sourced by vertical ground motion) with those observed by video analysis of CCTV camera records at the Pantoloan station.

3.3 Cardiovascular hemodynamics

Modeling of blood flow in the aortic system is a complex fluid-structure interaction (FSI) problem that is important to resolve in order to develop a better understanding of the underlying mechanisms of cardiovascular diseases such as aneurysms and heart failure. It is also an essential tool in the design and performance evaluation of cardiovascular devices such as artificial heart valves, stents and grafts. The pulsatile flow that is generated in the heart can be modeled as pressure and flow waves as it enters the (compliant) aorta and reflects through vasculature due to vessel tapering (thinning), bifurcations and variations in arterial wall elastic material properties. These multiphysical dynamics can be studied to provide assessment of cardiac health.

In order to simulate the complete circulation with, in particular, the different material properties encountered in various vascular segments, it is necessary to adopt a nonlinear and physiologically-relevant fluid-structure model. For cross-sectional area $A = A(x,t)$ and mean velocity over the cross-section $U = U(x,t)$ (yielding the flow rate as $Q = AU$), such a model can be expressed as a reduced-order nonlinear system for each segment as

$$\begin{pmatrix} \dfrac{\partial A}{\partial t}(x,t) \\ \dfrac{\partial U}{\partial t}(x,t) \end{pmatrix} = - \begin{pmatrix} \dfrac{\partial (AU)}{\partial x}(x,t) \\ U\dfrac{\partial U}{\partial x}(x,t) + \dfrac{1}{\rho}\dfrac{\partial P}{\partial x}(x,t) + \dfrac{2(\zeta+2)\mu\pi U(x,t)}{\rho A(x,t)} \end{pmatrix}, \tag{10}$$

where ρ is a (constant) blood density, μ is a (constant) blood viscosity and ζ is a given constant of an assumed axisymmetric velocity profile. The system is closed by an assumed nonlinear elastic *tube law* that accounts for the fluid-structure interaction and is given by the constitutive law

$$P(x,t) - P_{\text{ext}} = P_{\text{d}} + \frac{\beta}{A_{\text{d}}}\left(\sqrt{A(x,t)} - \sqrt{A_{\text{d}}}\right), \quad \beta(x) = \frac{4}{3}\sqrt{\pi}E(x)h(x), \tag{11}$$

where $P_{\text{ext}}(x)$ is the external pressure, $P_{\text{d}}(x)$ is the diastolic pressure, $A_{\text{d}}(x)$ is the diastolic area, and $\beta(x)$ is an expression of the arterial wall material properties in terms of elastic modulus $E(x)$ (a measure of stiffness) and wall thickness $h(x)$. In order to simulate multiple vessels, including vascular bifurcations or trifurcations, it is necessary to treat the fractal structure of the circulation network and, namely, branching points. These *junctions* effectively act as mathematical discontinuities in cross-sectional area and material properties. Physically, one must enforce a continuity of total pressure and a conservation of mass at each

junction point. For example, given a *parent* vessel p that splits into two *daughter* vessels $d,i=1,2$, the corresponding mathematical conditions are given by

$$P_p+\frac{\rho}{2}U_p^2=P_{d,i}+\frac{\rho}{2}U_{d,i},\quad i=1,2\quad\text{and}\quad A_pU_p+A_{d,1}U_{d,1}+A_{d,2}U_{d,2}=0. \tag{12}$$

Numerically, these equations are implemented through the solution of a corresponding *Riemann invariant* problem that enforces compatibility of propagating characteristics and provides the final three equations given by

$$w_{1p}=U_p+4A_p^{1/4}\sqrt{\frac{\beta_p}{2\rho}}\quad\text{and}\quad w_{2d,i}=U_{d,i}-4A_{2d,i}^{1/4}\sqrt{\frac{\beta_{d,i}}{2\rho}},\quad i=1,2, \tag{13}$$

where w_{1p} represents the outgoing characteristic from the parent vessel and $w_{2d,i}$ the outgoing characteristic from the daughter vessels (A and U can both be represented at the boundary in terms of both incoming and outgoing characteristics). The inlet and outlet boundary conditions for the aorta and terminal vessels, respectively, create highly nonlinear and nonstationary systems as they are governed by dynamic ODEs representing the heart and truncated vasculature [8, 9].

The FC-based solver (which has been extensively benchmarked [9] against those problems proposed in [11]) quickly resolves many-cycle cardiac simulations and clinical metrics with greater speed and accuracy [8, 9] than commonly used finite difference, finite volume and discontinuous Galerkin finite element methods (left Figure 4). Using these types of reduced-order models, it has been demonstrated [1] that a possible mechanical link exists between aortic arch stiffening of the elastic wall (which can be offset due to aging, smoking or diseases like type-2 diabetes) and excessive energy transmission to the brain (a possible indicator of dementia and Alzheimer's). An example of the pressure at the midpoint of the right common carotid artery (which goes towards the brain) is given in Figure 4 (right) and produced by a simulation of 77 segments of the human circulation [9]. In order to investigate such links fully, the FC-based solvers with dynamic heart models [8, 9] are necessary in order to study the effects of various heart conditions and properties (such as left ventricle contractility [9]). Recent efforts [1] have involved investigating whether certain "optimum wave conditions" exist in the cardiovascular system where harmful effects may be minimized.

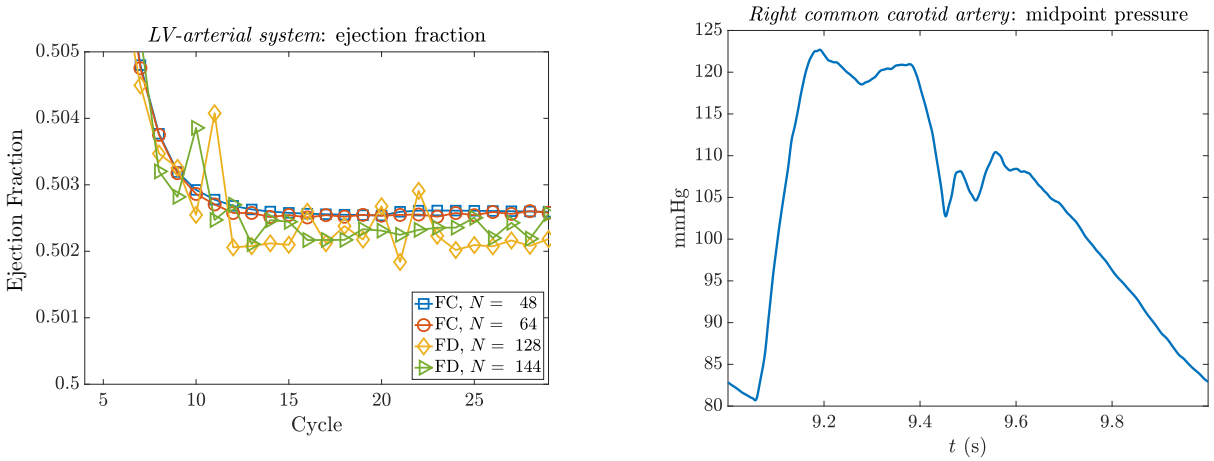

FIGURE 4 – Left : ejection fractions versus cardiac cycle (used in clinical practice for measuring heart failure) from [8], computed by a new FC-based solver (using a dynamic heart model) compared to those computed by commonly-used finite differences (FD). Right : pressure at the midpoint of the right common carotid artery simulated by a 77-segment circulatory system model [9].

4 Conclusions

This contribution presents an overview of recent developments in Fourier continuation-based numerical PDE methods motivated by treatment of (linear) elastodynamics equations, (nonlinear) shallow water wave equations and (nonlinear) fluid-structure hemodynamics equations with realistic sources and boundary conditions. Such solvers have enabled scientific computing applications that have provided mutual

validation of both simulation and data (natural or experimental) for problems in materials characterization, geophysics and cardiovascular medicine. Current ongoing efforts include stronger coupling with other models/methods (where challenges include the numerical representation of interfaces and efficient information transfer) ; the development of FC-adapted automated structured grid generation algorithms (e.g., those based on solutions of elliptic PDEs) ; the development of absorbing boundary conditions (where a preliminary formulation, based on the overset grid methodology, has been introduced in [4] but not yet fully explored) ; hybrid implicit-explicit time discretizations ; and GPU implementations of the FC procedure (whose FFT-based calculations are ideally suited for such architectures).

Références

[1] A. Aghilinejad, F. Amlani, K.S. King, N.M. Pahlevan. *Dynamic effects of aortic arch stiffening on pulsatile energy transmission to cerebral vasculature as a determinant of brain-heart coupling*, Scientific Reports, 10, 8784, 2020.

[2] N. Albin, O.P. Bruno. *A spectral FC solver for the compressible Navier-Stokes equations in general domains 1 : Explicit time-stepping*, Journal of Computational Physics, 230(16), 6248–6270, 2011.

[3] N. Albin, O.P. Bruno, T.Y. Cheung, R.O. Cleveland. *Fourier continuation methods for high-fidelity simulation of nonlinear acoustic beams*, The Journal of the Acoustical Society of America, 132(4), 2371–2387, 2012.

[4] F. Amlani. *A new high-order Fourier continuation-based elasticity solver for complex three-dimensional geometries*, PhD thesis, California Institute of Technology, 2014.

[5] F. Amlani, H.S. Bhat, W.J.F. Simons, A. Schubnel, C. Vigny, A.J. Rosakis, J. Efendi, A. Elbanna, H.Z. Abidin. *Supershear shock front contributions to the tsunami from the 2018 M_w 7.5 Palu earthquake*, under review (arXiv preprint arXiv :1910.14547), 2021.

[6] F. Amlani, O.P. Bruno. *An FC-based spectral solver for elastodynamic problems in general three-dimensional domains*, Journal of Computational Physics, 307, 333–354, 2016.

[7] F. Amlani, O.P. Bruno, J.C. López-Vázquez, C. Trillo, Á.F. Doval, JL Fernández, P Rodríguez-Gómez. *Transient propagation and scattering of quasi-Rayleigh waves in plates : quantitative comparison between pulsed TV-holography measurements and FC(Gram) elastodynamic simulations*, arXiv preprint, arXiv :1905.05289, 2019.

[8] F. Amlani, N.M. Pahlevan. *A stable high-order FC-based methodology for hemodynamic wave propagation*, Journal of Computational Physics, 405, 109130, 2020.

[9] F. Amlani, N.M. Pahlevan. *A novel Fourier-based (pseudo) spectral framework for 1D hemodynamics and wave propagation in the entire human circulatory system*, Bulletin of the American Physical Society 66, 2021.

[10] F. Amlani, H. Wei, N.M. Pahlevan. *A new psuedo-spectral methodology without numerical diffusion for conducting dye simulations and particle residence time calculations*, under review (arXiv preprint arXiv :2112.05257), 2021.

[11] E. Boileau, P. Nithiarasu, P.J. Blanco, L.O. Müller, F.E. Fossan, L.R. Hellevik, W.P. Donders, W. Huberts, M. Willemet, J. Alastruey. *A benchmark study of numerical schemes for one-dimensional arterial blood flow modelling*, International Journal for Numerical Methods in Biomedical Engineering, 31(10), p.e02732, 2015.

[12] J.P. Boyd, J.R. Ong. *Exponentially-convergent strategies for defeating the Runge phenomenon for the approximation of non-periodic functions, part I : single-interval schemes*, Communications in Compututational Physics, 5(2-4), 484–497, 2009.

[13] O.P. Bruno, M. Lyon. *High-order unconditionally stable FC-AD solvers for general smooth domains 1. Basic elements*, Journal of Computational Physics, 229(6), 2009–2033, 2010.

[14] M. Fontana, O.P. Bruno, P.D. Mininni, and P. Dmitruk. *Fourier continuation method for incompressible fluids with boundaries*, Computer Physics Communications, 256, 107482, 2020.

[15] E.L. Gaggioli, O.P. Bruno, D M. Mitnik. *Light transport with the equation of radiative transfer : The Fourier Continuation–Discrete Ordinates (FC–DOM) Method*, Journal of Quanti- tative Spectroscopy and Radiative Transfer, 236, 106589, 2019.

[16] J.C. López-Vázquez, L.D.B. Xosé, C. Trillo, Á.F Doval, J.L. Fernandez, F. Amlani, O.P. Bruno. *Numerical modeling and measurement by pulsed television holography of ultrasonic displacement maps in plates with through-thickness defects*, Optical Engineering, 49(9), 095802, 2010.

[17] N.M. Pahlevan, F. Amlani, K.S. King, A. Aghilinejad. *The Effects of Left Ventricle Contractility on Aortic-Brain Hemodynamic Coupling*, Bulletin of the American Physical Society 66, 2021.

[18] K. Shahbazi, J.S. Hesthaven, and X. Zhu. *Multi-dimensional hybrid Fourier continuation-WENO solvers for conservation laws*, Journal of Computational Physics, 253, 209–225, 2013.